https://doi.org/10.15407/ujpe66.6.518

A.V. KOROTUN, A.O. KOVAL, V.V. POGOSOV
Zaporizhzhya National Technical University
(64, Zhukovs'kogo Str., Zaporizhzhya 69063, Ukraine; e-mail: andko@zntu.edu.ua)

OPTICAL PARAMETERS OF BIMETALLIC NANOSPHERES

A formula for the relaxation time of electrons at the surface of a sphere consisting of a metal core and a metal shell (core-shell) has been derived and the frequency dependences of the electric and magnetic components of the sphere polarizability have been analyzed. The sphere polarization maxima correspond to the plasmon resonances of the core and the shell. Calculations are carried out for bimetallic Ag–Au, Au–Ag, and Ag–Al nanoparticles embedded in Teflon. A possibility to control the optical characteristics of bimetallic nanoparticles by changing their morphology is demonstrated. The extinction and scattering cross-sections and the field enhancement factor in the nanoparticle vicinity are calculated in a wide spectral interval and for various core-to-shell size ratios. The temperature of a photothermally heated bimetallic nanosphere used for the therapy of malignant tumors is evaluated.

K e y w o r d s: bimetallic nanoparticle, dipole polarizability, dielectric function, surface plasmon, field enhancement factor.

1. Introduction

The current level of technology makes it possible to create nanostructures with controlled optical parameters. Such systems, in turn, may exhibit unexpected properties when reflecting and absorbing light.

The research of metal nanoparticles is of interest because of their wide application in photo- and electrocatalysis, as sensors in biology and medicine, and so forth [1–8]. Such a variety of potential nanoparticle applications is possible, first of all, due to the appearance of a plasmon resonance. The shape and position of the plasmon resonance peak depend on the particle size and shape, as well as on the heterogeneity of particle conglomerates [1, 9, 10]. Therefore, those parameters can be adjusted by selecting the corresponding synthesis conditions, which is especially important for creating the information processing devices and for the development of subwavelength optical devices, plasmon nanoantennas, and nanolasers, as well as elements of optical schemes and photodetectors [11].

The interaction of electromagnetic fields with metal nanoparticles, especially at the frequencies near the plasma resonance, is known to result in the enhancement of the field both inside the particle and in its environment, as well as in the enhancement of light scattering and absorption by the particle [12–15]. All those features are associated with the resonances in the dipole polarizability $\alpha(\omega)$ of the particle. For a sphere of radius R embedded into a dielectric matrix with the dielectric permittivity $\epsilon_{\rm m}$, the expression for the dipole polarizability looks like

$$\tilde{\alpha} \equiv \frac{\alpha}{R^3} = \frac{\epsilon - \epsilon_{\rm m}}{\epsilon + 2\epsilon_{\rm m}}, \tag{1}$$

where ϵ is the dielectric function of the sphere. Knowing the polarizability, one can determine the cross-sections of light absorption, $C^{\rm abs}$, and scattering, by the particle. Those quantities, being experimentally measurable, are of the largest interest. In particular, the scattering cross-section can be measured in dark-field experiments, and the sum of both cross-sections (the extinction cross-section) can be found by measuring the light transmission.

In the framework of the dipole approximation for monometallic spheres, the absorption, $C^{\rm abs}$, and scattering, $C^{\rm sca}$, cross-sections are determined in terms of the electric, α, and magnetic, $\alpha^{\rm mag}$, polarizabilities as follows [1, 16, 17]:

$$Q^{\rm abs} = \frac{C^{\rm abs}}{\pi R^2}, \; C^{\rm abs} = \frac{4\pi\omega}{c}\epsilon_{\rm m}^{1/2}\,{\rm Im}(\alpha + \alpha^{\rm mag}), \tag{2}$$

$$Q^{\rm sca} = \frac{C^{\rm sca}}{\pi R^2},\ C^{\rm sca} = \frac{\omega^4 \epsilon_{\rm m}^2}{6\pi c^4} |\alpha + \alpha^{\rm mag}|^2, \tag{3}$$

The dimensionless quantities

$$Q^{\rm abs} = \frac{C^{\rm abs}}{\pi R^2}$$

and

$$Q^{\rm sca} = \frac{C^{\rm sca}}{\pi R^2}$$

are called the absorption and scattering efficiencies, respectively. In formulas (2) and (3), c is the speed of light, and the expression for $\alpha^{\rm mag}$ reads

$$\alpha^{\rm mag} = \left(\frac{\omega R}{c}\right)^2 \epsilon_{\rm m} \frac{R^3}{30} (\epsilon - \epsilon_{\rm m}). \tag{4}$$

provided that

$$\frac{\omega R}{c} |\epsilon_{\rm m} \epsilon_{@}(\omega)|^{1/2} \ll 1.$$

In the infrared spectral interval, the contribution of $\mathrm{Im}\, \alpha^{\rm mag}$ in Eqs. (2) and (3) increases with the particle radius R, and the values of the quantities $\mathrm{Im}\, \alpha$ and $\mathrm{Im}\, \alpha^{\rm mag}$ become approximately equal to each other at $R \approx 2$ nm [16].

The enhancement factor $\mathscr{G}$ for the field near a monometallic nanoparticle is calculated by the formula

$$\mathscr{G}(r) = \left|1 + 2\alpha / r^3\right|^2, \tag{5}$$

where $r > R$ is the distance from the sphere center to the point, where the field enhancement factor is determined [1,18] (see Fig. 1 for a bimetallic sphere).

Provided that the quantum size effects are neglected for the dielectric function of a metal particle, the modified Drude theory can be used, and

$$\epsilon = \epsilon^{\infty} - \frac{\omega_{bp}^2 \tau^2}{1 + \omega^2 \tau^2} + \mathrm{i} \frac{\omega_{bp}^2 \tau}{\omega (1 + \omega^2 \tau^2)}. \tag{6}$$

Here, $\mathrm{i} = \sqrt{-1}$; ϵ^{∞} is the "zero-point term" describing the contribution of the metal ion core; $\omega_{bp} = \left[\bar{n} e^2 / (\epsilon_0 m^*)\right]^{1/2}$ is the bulk plasma frequency; ϵ_0 is the dielectric constant; $\bar{n}$, m^*, and τ are the concentration, effective mass, and relaxation time of electrons, respectively; $\bar{n}^{-1} = 4\pi \bar{r}^3/3$; and $\bar{r}$ is the average distance between the conduction electrons.

If the characteristic sizes become smaller than the free path length of electrons, besides the scattering of electrons at phonons, impurities, and other defects, their scattering at the sphere surface must be taken into consideration. For monometallic spheres, the time τ in Eq. (6) is substituted by the effective relaxation time $\tau^{\rm eff}$. The latter is determined by the formula

$$\frac{1}{\tau^{\rm eff}} = \frac{1}{\tau^{\rm bulk}} + \frac{1}{\langle l \rangle_R / v_{\rm F}}, \tag{7}$$

where $\tau^{\rm bulk}$ is the relaxation time in the 3D metal, $\langle l \rangle_R$ is the average free path length of electrons in the sphere between their scattering at the sphere surface, and

$$v_{\rm F} = \frac{\hbar}{m^*} \left(3\pi^2 \bar{n}\right)^{1/3}, \tag{8}$$

is the Fermi velocity of electrons. The classical approach can be applied to describe the electron scattering, if $\hbar\omega \ll \varepsilon_{\rm F}$.

The following relation is often used in the literature:

$$\frac{1}{\langle l \rangle_R / v_{\rm F}} \equiv \frac{\mathscr{A}}{R / v_{\rm F}}, \tag{9}$$

where $\mathscr{A}$ is an effective parameter that characterizes the degree of coherence loss, when an electron is scattered at the surface [12–14]. For instance, $\mathscr{A} = 1$ for the classical diffuse scattering regime [12], and $\mathscr{A} = 3/4$ for the isotropic one (see also Fig. 4 in work [15], where the dependence $\mathscr{A}(\omega, R)$ was calculated for Ag nanoparticles and compared with experimental data).

After the publication of the famous book [19], in which the optical size-dependent properties of monometallic clusters located in various matrices were analyzed, there appeared only a few reports on the results of new measurements in the literature, most likely because of the complicated character of experiments [20–22]. Interest in the early works was mainly focused on the absorption by metal particles in the far-infrared spectral interval (see, e.g., works [16,17] and the references therein). Nowadays, the focus of research is aimed at nanoplasmonics, which is associated, first of all, with its applications in biology and medicine.

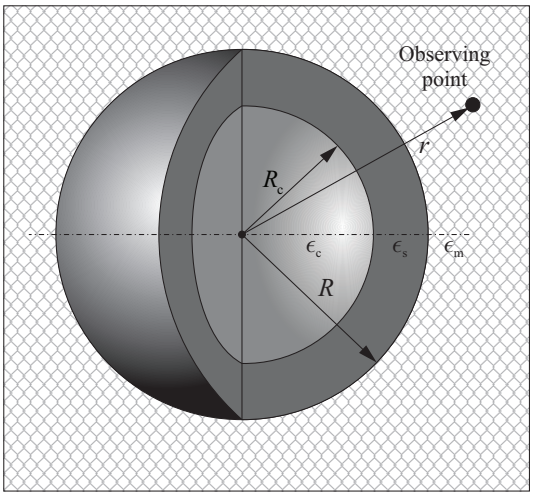

Fig. 1. Schematic diagram of a bimetallic sphere and the notations used for its parameters

The frequency of surface plasmons ω_{sp} in a monometallic sphere is determined from the condition that the real part of the denominator in expression (1) for $\alpha(\omega)$ should equal zero. As a result, we obtain

$$\omega_{sp} = \sqrt{\frac{\omega_{bp}^2}{\epsilon^{\infty} + 2\epsilon_{\rm m}} - \left(\frac{1}{\tau^{\rm bulk}} + \mathscr{A}\frac{v_{\rm F}}{R}\right)^2}. \tag{10}$$

The core-shell (A-B) structures–in particular, bimetallic particles [22–27]–are characterized by a shift in the plasmon resonance frequency as compared with that for monometallic particles. Owing to differences in the light scattering and absorption by atoms of different metals, the parameters of surface plasmon resonance depend on the sizes and materials of the core and the shell and can vary in a wider spectral interval. This circumstance, in turn, favors the enhancement of the photothermal response of the structures concerned to laser irradiation [28, 29], which is already used for the development of nanotechnological methods of cancer treatment [30].

Thus, the purposeful control depending on the needs, over the parameters of bimetallic nanoparticles can lead to a substantial improvement of the properties and the efficiency of materials fabricated on their basis. Therefore, the research of the optical characteristics of bimetallic nanoparticles and the analysis of how those properties can be controlled by changing the composition and geometric parameters of the nanoparticle core and shell comprise a challenging task because of wide prospects of the nanoparticle application in practice.

2. Basic Relations

Let us consider a bimetallic sphere with radius R embedded into a dielectric matrix with the dielectric permittivity $\epsilon_{\rm m}$. The shell of thickness t covers a core of the radius $R_{\rm c}$ so that $R_{\rm c} + t = R$ (Fig. 1). The dipole polarizability $\tilde{\alpha}_{@}$ of this sphere can be written as follows [31, 32]:

$$\tilde{\alpha}_{@} = \frac{(\epsilon_{\rm s} - \epsilon_{\rm m})(2\epsilon_{\rm s} + \epsilon_{\rm c}) - (2\epsilon_{\rm s} + \epsilon_{\rm m})(\epsilon_{\rm s} - \epsilon_{\rm c})\beta_c}{(\epsilon_{\rm s} + 2\epsilon_{\rm m})(2\epsilon_{\rm s} + \epsilon_{\rm c}) - 2(\epsilon_{\rm s} - \epsilon_{\rm m})(\epsilon_{\rm s} - \epsilon_{\rm c})\beta_c} \equiv$$

$$\equiv \alpha_{@}/R^3, \tag{11}$$

where the parameters $\tilde{\alpha}_{@}, \epsilon_{\rm s}$, and $\epsilon_{\rm c}$ depend on the light frequency ω, and $\beta_{\rm c} = R_{\rm c}^3/R^3$ is the volume fraction of the core material in the bimetallic spherical nanoparticle. The parameter $\beta_{\rm c}$ always acquires values within an interval of (0,1). If $R_{\rm c} = 0$ or $t = 0$, i.e. $\beta_{\rm c} = 0$ or 1, respectively, then the sphere becomes monometallic ($\epsilon_{\rm s} = \epsilon_{\rm c} \equiv \epsilon$), and expressions (11) and (1) are identical.

By analogy with Eq. (1), expression (11) can be written in a more compact form,

$$\tilde{\alpha}_{@} = \frac{\epsilon_{@} - \epsilon_{\rm m}}{\epsilon_{@} + 2\epsilon_{\rm m}}, \tag{12}$$

thus introducing the dielectric constant of the two-layer sphere

$$\epsilon_{@} = \epsilon_{\rm s}\frac{1 + 2\beta_{\rm c}\delta_{@}}{1 - \beta_{\rm c}\delta_{@}}, \tag{13}$$

where

$$\delta_{@} \equiv \frac{\epsilon_{\rm c} - \epsilon_{\rm s}}{\epsilon_{\rm c} + 2\epsilon_{\rm s}}.$$

Following the style of the Drude theory [Eqs. (6) and (7)], let us express the complex dielectric function of the core(shell) in the form

$$\epsilon_{\rm c(s)} = \epsilon_{\rm c(s)}^{\infty} - \frac{\omega_{bp,\,{\rm c(s)}}^2 \left(\tau_{\rm c(s)}^{\rm eff}\right)^2}{1 + \omega^2\left(\tau_{\rm c(s)}^{\rm eff}\right)^2} +$$

$$+ {\rm i}\frac{\omega_{bp,\,{\rm c(s)}}^2 \tau_{\rm c(s)}^{\rm eff}}{\omega\left[1 + \omega^2\left(\tau_{\rm c(s)}^{\rm eff}\right)^2\right]}, \tag{14}$$

where

$$\frac{1}{\tau_{\rm c}^{\rm eff}} = \frac{\beta_{\rm c}}{\tau_{\rm c}^{\rm bulk}}, \quad \frac{1}{\tau_{\rm s}^{\rm eff}} = \frac{(1-\beta_{\rm c})}{\tau_{\rm s}^{\rm bulk}} + \frac{1}{\left\langle \tau_{@}^{\rm surf} \right\rangle_R}, \tag{15}$$

and determine the average mean free time $\left\langle \tau_{@}^{\rm surf} \right\rangle_R = \left\langle l/v_{\rm F} \right\rangle_R$ in the form corresponding to the case of diffuse scattering. The expression for the probability of the electron scattering at angles within the intervals $(\theta, \theta + d\theta)$ and $(\varphi, \varphi + d\varphi)$ with respect to the tangent plane of the sphere (Fig. 2) looks like

$$dW = W_0 \cos\theta \, d\theta \, d\varphi,$$

where $\theta \in (0, \pi/2)$ and $\varphi \in (0, 2\pi)$. Finally, the average relaxation time at the surface is defined by the formula

$$\left\langle \tau_{@}^{\rm surf} \right\rangle_R = \frac{\int \tau_{@}^{\rm surf} \, dW}{\int dW}. \tag{16}$$

Then, for the "subcritical" angles $\theta \leq \theta^*$, where $\cos\theta^* = R_{\rm c}/R$, an electron is scattered only in the shell, whereas at $\theta > \theta^*$, it can be scattered in both the shell and the core (two different metals). In this connection, let us write $\left\langle \tau_{@}^{\rm surf} \right\rangle_R$ in the form

$$\left\langle \tau_{@}^{\rm surf} \right\rangle_R = \int\limits_0^{\theta^*} \frac{2R\sin\theta}{v_{\rm F,s}} \cos\theta d\theta + \\ + \int\limits_{\theta^*}^{\pi/2} \left(\frac{l_1}{v_{\rm F,s}} + \frac{l_2}{v_{\rm F,c}} + \frac{l_3}{v_{\rm F,s}} \right) \cos\theta d\theta. \tag{17}$$

For the parameter l_1, by solving the geometric problem, we obtain the quadratic equation

$$l_1^2 = R_{\rm c}^2 - R^2 + 2 l_1 R \sin\theta.$$

Its solution equals

$$l_1 = R\sin\theta - \sqrt{R_{\rm c}^2 - R^2\cos^2\theta}.$$

Analogously, for the parameters l_2 and l_3, we obtain

$$l_2 = \frac{R^2 - R_{\rm c}^2 - l_1^2}{l_1},$$

$$l_3 = 2R\sin\theta - l_2 - l_1.$$

In the case of monometallic sphere – for instance, if we put $(R_{\rm c}, \beta_{\rm c}) \to 0$ – we arrive at expressions (6), (7), and $\left\langle l/v_{\rm F} \right\rangle_R = R/v_{\rm F}$.

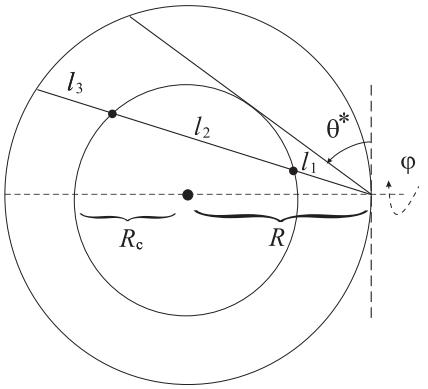

Fig. 2. Geometry of the electron scattering in a bimetallic sphere

Now, integrating in Eq. (17) and accounting for the expressions obtained for l_1, l_2, and l_3, we finally obtain

$$\left\langle \tau_{@}^{\rm surf} \right\rangle_R = \frac{R}{\mathscr{A} v_{\rm F,s}}, \tag{18}$$

where

$$\frac{1}{\mathscr{A}} = 1 + \left(\frac{v_{\rm F,s}}{v_{\rm F,c}} - 1 \right) \times \\ \times \left[\beta_{\rm c}^{1/3} - \frac{1}{2} \left(1 - \beta_{\rm c}^{2/3} \right) \ln \left(\frac{1 + \beta_{\rm c}^{1/3}}{1 - \beta_{\rm c}^{1/3}} \right) \right].$$

3. Calculation Results and Their Discussion

By analogy with the case of monometallic spheres [formulas (1)–(9)], let us calculate the frequency dependences of the polarizability, the absorption and scattering efficiencies, and the field enhancement factor for bimetallic Ag–Au, Au–Ag, and Ag–Al spheres embedded into Teflon ($\epsilon_{\rm m} = 2.3$) using the direct substitutions of the corresponding quantities [formulas (12)-(18)]. The parameter values for the examined metals are quoted in Table.

Parameter values for various metals [$a_0 = \hbar^2/(m_e e^2)$ is the Bohr radius]

Parameters	Al	Au	Ag
$\bar{r}$, a_0 [35]	2.07	3.01	3.02
m^*/m_e [10]	1.48	0.99	0.96
ϵ^∞ [10]	0.7	9.84	3.7
$\tau^{\rm bulk}$, 10^{-14} c [35]	8	29	40

In the case of a bimetallic sphere, there arises a potential difference at the interface between different metals owing to the flow of ΔN electrons between them, which equalizes the chemical potentials of electrons in both metals. As a result, the bottoms of the conduction bands in the metals become shifted. As a rule, the thickness of the contact layer is equal to several Bohr radii. Therefore, the abrupt change in the velocity of a classical scattered particle (its charge does not matter at that) is a model feature and has no physical consequences.

Let us consider the influence of the contact between the metals on the electron velocity. For this purpose, let us conditionally divide the bimetallic sphere into two clusters (a solid core and a hollow shell, which are made of different metals), and let those clusters be located at a large distance from each other in an insulator with the dielectric permittivity $\epsilon_{\rm m}$. Neglecting the quantum-size effects, the work required to transfer ΔN electrons from either cluster into the insulator (ionization) and then into the other cluster (sticking) can be found. The energy of electrons is reckoned from their energy level in the insulator. As a result, we obtain the equalization condition for the chemical potentials of electrons in those clusters,

$$-|W_{\rm s} - W_{\rm c}|\Delta N + \frac{(e\Delta N)^2}{2}\left(\frac{1}{C_{\rm s}} + \frac{1}{C_{\rm c}}\right) = 0, \qquad (19)$$

where $W_{\rm s(c)}(\epsilon_{\rm m})$ is the work function for the semiinfinite metal the shell(core) is made of, possessing the flat surface, and contacting with the semiinfinite insulator (therefore, this parameter depends on $\epsilon_{\rm m}$ [33]), whereas $C_{\rm s}$ and $C_{\rm c}$ are the electric capacitances of both clusters embedded into the insulator [34]. The last terms in Eq. (19) is the charging energy of two clusters with the capacitances $C_{\rm s}(\epsilon_{\rm m})$ and $C_{\rm c}(\epsilon_{\rm m})$. As a result, we obtain

$$\Delta N = \frac{8\pi\epsilon_0\epsilon_{\rm m}RR_{\rm c}|W_{\rm s} - W_{\rm c}|}{e^2(R + R_{\rm c})}. \qquad (20)$$

Due to the contact, the electron concentrations in the core and the shell change together with the Fermi velocities in those metals. For example, if $W_{\rm c} > W_{\rm s}$, then, according to Eq. (8),

$$\frac{v_{\rm F,c}^3}{v_{\rm F,s}^3} = \frac{m_s^*}{m_c^*}\left(\frac{1}{\beta_{\rm c}} - 1\right)\frac{N_{\rm c} + \Delta N}{N_{\rm s} - \Delta N}, \qquad (21)$$

where $N_{\rm c}$ and $N_{\rm s}$ are the numbers of conduction electrons in the neutral core and shell, respectively, i.e. before the core and shell recharging.

Let us make some estimates. For example, using the values $R_{\rm c} = 10$ nm, $t = 5$ nm, $\beta_{\rm c} \approx 0.3$, $W_{\rm c} = 4.52$ eV, and $W_{\rm s} = 5.10$ eV for Ag–Au particles, we obtain $N_{\rm c} = R_{\rm c}^3/\bar{r}_{\rm c}^3 = 2.11 \times 10^5$, $N_{\rm s} = (R^3 - R_{\rm c}^3)/\bar{r}_{\rm s}^3 = 5.08 \times 10^5$, and $\Delta N \approx 11 \ll (N_{\rm c}, N_{\rm s})$. For the values $R_{\rm c} = 20$ nm and $t = 20$ nm, we have $N_{\rm c} = 1.7 \times 10^6$, $N_{\rm s} = 1.2 \times 10^7$, and $\Delta N \approx 24$. Therefore, since $\Delta N \ll (N_{\rm c}, N_{\rm s})$, the contact effect in Eq. (21) can be neglected.

Figures 3 and 4 illustrate the frequency dependences of the real and imaginary parts, as well as the absolute value, of the electric and magnetic components of the polarizability of the spherical Ag–Au nanospheres with various sizes. Note that the function $\mathrm{Re}\,\tilde{\alpha}_@(\omega)$ is alternating, whereas $\mathrm{Im}\,\tilde{\alpha}_@(\omega) > 0$ in the whole frequency interval. In addition, the growth of the core radius (the increase of the Ag fraction in the nanoparticle) results in a reduction of the distance between the maxima of $\mathrm{Re}\,\tilde{\alpha}_@$, $\mathrm{Im}\,\tilde{\alpha}_@$, and $|\tilde{\alpha}_@|$, and the increase of their magnitudes. Furthermore, the second maxima of $\mathrm{Im}\,\tilde{\alpha}_@$ and $|\tilde{\alpha}_@|$ become more pronounced. The polarizability maxima correspond to the plasmon resonances in the core and the shell.

On the basis of expression (10) for the frequency of surface plasmons in a monometallic sphere, one may expect a red shift of the plasma frequency when the sphere radius R decreases. However, as follows from Fig. 3, if $R_{\rm c}$ decreases, and if the shell thickness t remains constant, i.e. the total cluster radius R decreases, the red shift of the first resonance really takes place (the maxima of the curves in the sequence 3→2→1 are shifted to the left along the frequency axis). The red shift of the second resonance is also observed for the same curves, but it is much smaller.

At the same time, for the sequence $5 \to 4 \to 2$ of the curves (here, $R_{\rm c} = \mathrm{const}$ and t decreases, so that R decreases), the effect is opposite, i.e. a blue shift of the resonances is observed. Thus, as the radius of the sphere decreases, the resonances "repulse" each other.

Similar calculations carried out for the Au–Ag and Ag–Al nanoparticles with the same $R_{\rm c}$- and t-values resulted in the shift of all spectra (Fig. 3) toward high frequencies and the repulsion between the resonances. They also confirmed the indicated size-induced red and blue shifts of plasma resonances.

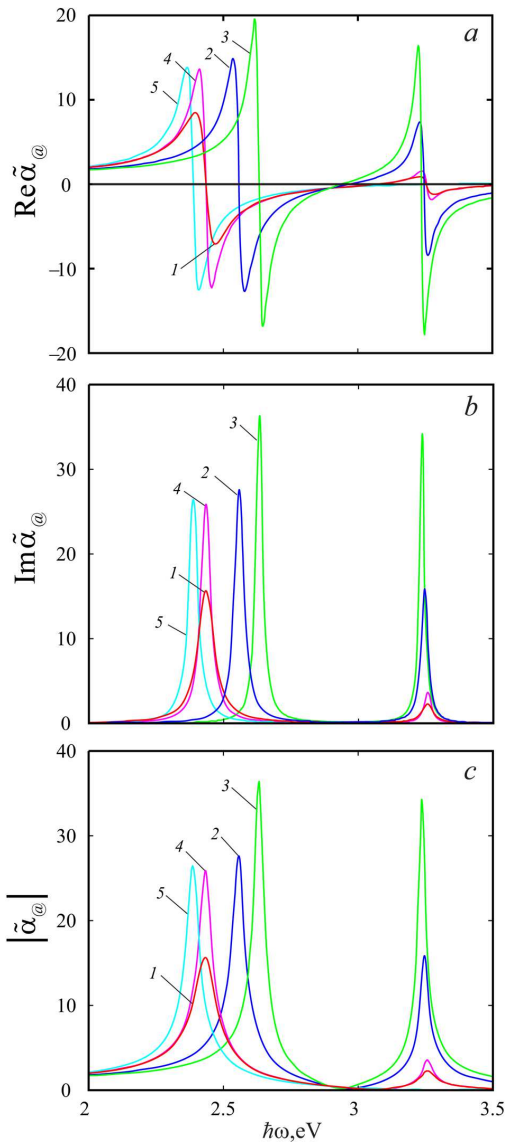

Fig. 3. Frequency dependences for the electrical component of the polarizability of Ag–Au spheres in Teflon. Curves *1*–*3*: the shell thickness $t = 5$ nm and the core radius $R_c = 10$ (*1*), 20 (*2*), and 30 nm (*3*). Curves *4* and *5*: the core radius $R_c = 20$ nm and the shell thickness $t = 10$ (*4*) and 20 nm (*5*)

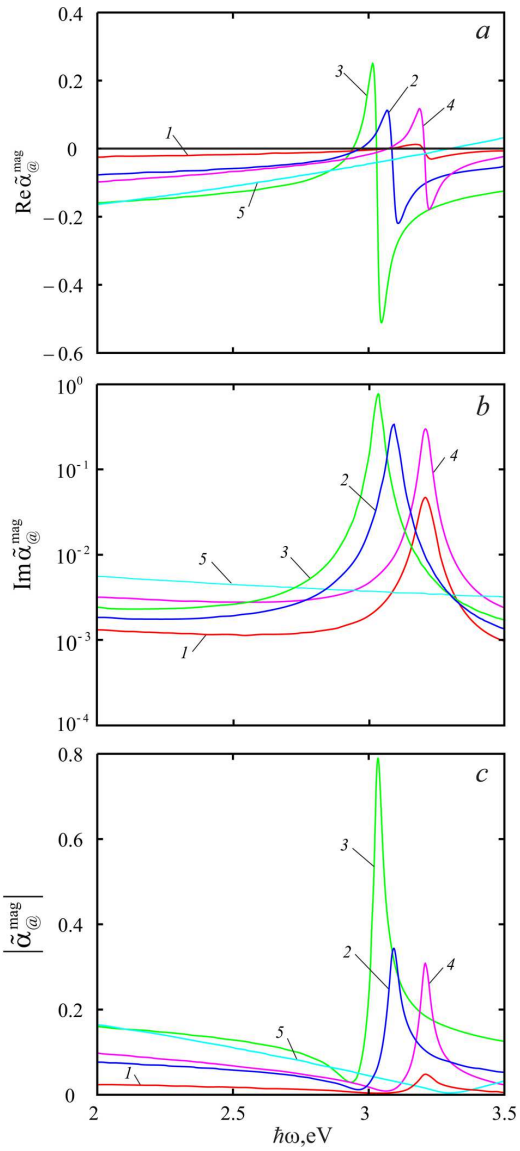

Fig. 4. Frequency dependences for the magnetic component of the polarizability of Ag–Au spheres in Teflon. The parameter values are the same as in Fig. 3

In order to determine the influence of the selected parameters, we also made calculations for the following parameters of the Drude theory: $\epsilon^{\infty} = 1$ and $m^*/m_e = 1$. As a result, the whole picture of resonances became shifted by about double frequencies, but the size-induced red and blue shifts did not change qualitatively.

Thus, formula (10) describes the resonances only partially. An analogous formula for a bimetallic sphere has to make allowance for a substantial number of metal parameters (see Table), as well as the radii of the core and the shell. Therefore, it is easier to perform the relevant analysis using numerical methods in this case.

Figure 4 demonstrates the frequency dependences of the magnetic polarizability of nanoparticles,

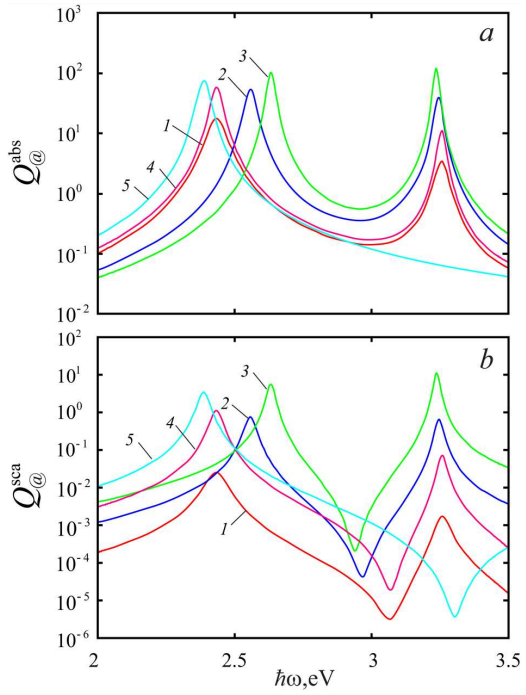

Fig. 5. Frequency dependences for the absorption and scattering efficiencies of Ag–Au spheres in Teflon. The parameter values are the same as in Fig. 3

$\alpha_@^{mag}(\omega)$. Their specific features are similar, in whole, to those shown in Fig. 3, but in accordance with formula (4). In the examined frequency interval, $\alpha_@^{mag}(\omega) \ll \alpha_@(\omega)$. But $\alpha_@^{mag}(\omega) \gg \alpha_@(\omega)$ in the far-infrared interval for a sphere with the indicated size. Those inequalities determine the main contribution of the electrical and magnetic components to the absorption efficiency.

The curves describing the frequency dependences of the absorption and scattering efficiencies are depicted in Figs. 5 and 6. Since $Q_@^{abs} \sim \mathrm{Im}\tilde{\alpha}_@$, the behavior of the curves $Q_@^{abs}(\omega)$ shown in Fig. 5, *a* is similar to that of the dependence $\mathrm{Im}\tilde{\alpha}_@\,(\omega)$. Furthermore, $Q_@^{sca} \ll Q_@^{abs}$ (see Fig. 5, *b*) so that $Q_@^{ext} \approx Q_@^{abs}$ and, therefore, the losses of the incident electromagnetic wave energy are mainly governed by absorption processes.

In Fig. 6, the frequency dependences of the absorption efficiency of bimetallic nanoparticles with the same size but with different elemental compositions are compared. Depending on which metal (Ag or Au) prevails in the nanoparticle, either the second or the first maximum is more pronounced. However, there are no $Q_@^{abs}\,(\omega)$-maxima in the studied frequency interval for the Ag–Al nanoparticles. Instead, the absorption efficiency increases with the growing frequency, which is especially noticeable for nanoparticles with larger Ag cores.

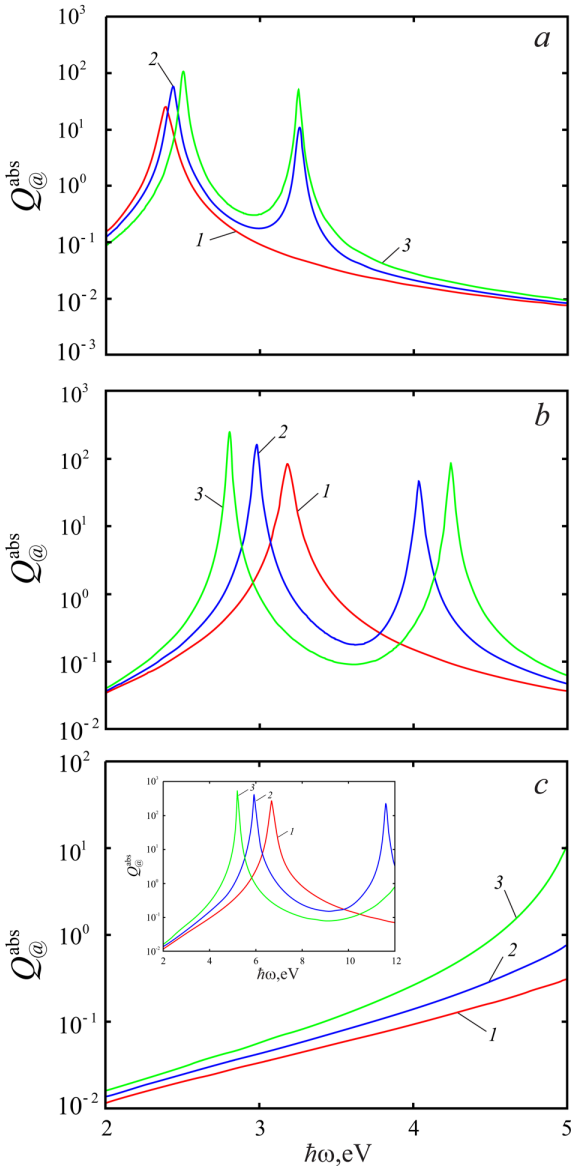

Fig. 6. Frequency dependences for the absorption efficiency of the Ag–Au (*a*), Au–Ag (*b*), and Ag–Al (*c*) nanoparticles with $t = 10$ nm and $R_c = 10$ (*1*), 20 (*2*), and 30 nm (*3*)

In Fig. 7, *a*, the frequency dependences of the field enhancement factor $\mathscr{G}$ for the Ag–Au nanoparticles with $R_c/R = 0.8$ are shown. One can see that this

quantity decreases as the distance from the nanoparticle surface increases, and its maximum $\mathscr{G}_{\max}$ is reached at $\hbar\omega \simeq 2.5$ eV irrespective of the distance from the nanoparticle surface. The influence of the elemental composition on the value of the field enhancement factor at the fixed value $R/r = 0.8$ is illustrated in Fig. 7, *b*. In this case, the maximum of the quantity $\mathscr{G}$ becomes shifted, which is a result of the change in the frequency of the surface plasmon resonance. Analogous dependences for the Ag–Au nanoparticles with various values of the ratio R_c/R are shown in Fig. 7, *c*. The reduction of the R_c/R-value leads to an increase of $\mathscr{G}_{\max}$ owing to the growth of the Au content in the nanoparticle.

An important application of nanoplasmonics is the photothermal therapy of malignant tumors. After the external pumping of light, the average temperature of the sphere rises by ΔT. Provided that the optimum temperature of the sphere should be 42°C, we obtain that $\Delta T = 42\ ^\circ\text{C} - 36.6\ ^\circ\text{C} = 5.4\ ^\circ\text{C}$.

The growth of the sphere temperature can be evaluated using the formula

$$\Delta T \approx \frac{I_0}{4\pi R\kappa} C_{@}^{\text{abs}} = \frac{I_0 R}{4\kappa} Q_{@}^{\text{abs}}, \tag{22}$$

where I_0 is the intensity of incident light, and κ the thermal conductivity of the environment [36]. Let us evaluate the temperature increase for a bimetallic Ag–Au nanoparticle with the parameters $R_c = 10$ nm and $t = 5$ nm embedded into a Teflon matrix ($\kappa = 0.25$ W/m/K and for the intensity $I_0 = 1$ mW/μm^2 of incident green light with the wavelength $\lambda = 530$ nm (the parameter values were taken from work [36]). According to Fig. 6, we have $Q_{@}^{\text{abs}} = 10$ at $\hbar\omega = 2.34$ eV, so that $\Delta T \approx 150\ ^\circ$C. If the nanoparticle is embedded into water ($\kappa = 0.6$ W/m/K and $\epsilon_{\text{m}} = 1.77$), then $\Delta T \approx 60^\circ$C. Such a temperature growth exceeds the necessary one by about an order of magnitude. However, it can be easily controlled by changing the parameters of the sphere and the distance r from it because the spatial temperature distribution looks like $\Delta T/r$ at $r > R$.

Figure 7 illustrates the results of calculation obtained for the field enhancement factor in the case of a single nanoparticle. For a conglomerate of nearby located spheres, there is a possibility to strengthen the external fields both inside and near the conglomerate by orders of magnitude. Therefore, we may assert that owing to this effect, the value of I_0 in formula (22) can be reduced by orders of magnitude, which, nevertheless, will be enough to achieve a required temperature for the treatment of malignant tumors. Perhaps, such therapy may probably occur

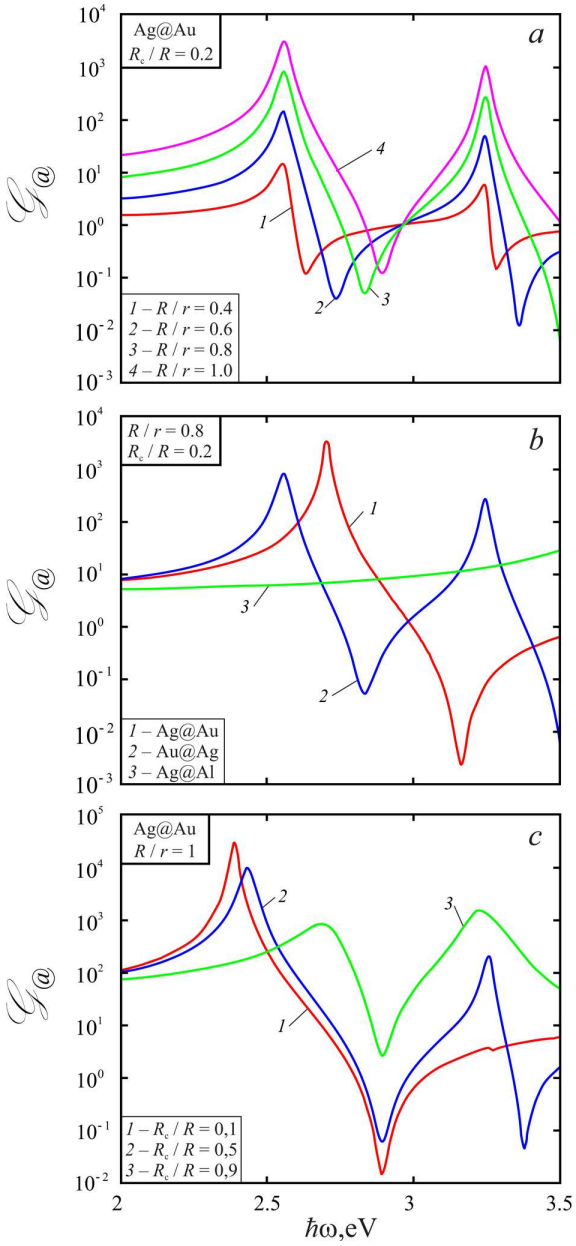

Fig. 7. Frequency dependences of the field enhancement factor (*a*) at various distances from the sphere surface for the Ag–Au spheres with $/R_c/R = 0.2$, (*b*) at $R/r = 0.8$ for spheres with $R_c/R = 0.2$ and various compositions, and (*c*) at the surface of the Ag–Au spheres with various R_c/R values

per se, i.e. without using a fixed external radiation source ($I_0 = 0$) but only due to weak random sources activated by the waves within the tissue transparency window.

4. Conclusions

The spectral dependences for the real and imaginary parts, as well as the absolute value, of the polarizability of a spherical bimetallic (core-shell) nanoparticle have been obtained. The frequency dependences of the polarizability and the absorption and scattering efficiencies are calculated for nanoparticles with various elemental compositions, core radii, and shell thicknesses.

In the case of Ag–Au nanoparticles, the first or the second maximum in the frequency dependences of the imaginary part and the absolute value of the nanoparticle polarizability turns out more pronounced depending on which metal prevails in the particle composition. The maxima themselves correspond to the plasmon resonances in the particle core or shell. If the core radius decreases and the shell thickness is fixed, i.e. the overall radius of the nanoparticle decreases, an appreciable red shift of the first resonance and a much smaller red shift of the second resonance take place. In the case where the core radius is constant and the shell thickness decreases, so that the outer radius of the cluster also decreases, a blue shift of resonances is observed. Thus, as the radius of the sphere decreases, the resonances "repulse" each other.

The scattering efficiency turns out much lower than the absorption efficiency at the same frequencies. Therefore, we may assume that the energy losses of the incident electromagnetic wave are mainly associated with absorption processes.

The behavior of the frequency dependences of the absorption efficiency substantially depends on the elemental composition of the nanoparticles. The corresponding curves for the Ag–Au and Au–Ag nanoparticles have two maxima in the examined spectral interval. But, for the Ag–Al nanoparticles, there are no maxima at those frequencies (see Fig. 6, *c*).

It is shown that the maximum position of the field enhancement factor is determined by the frequency of the surface plasmon resonance.

The temperature growth near bimetallic spheres located in various media due to absorption from external sources is evaluated. Note that there is a possibility to weakly heat the nanospheres in the radio frequency interval, which is favorable for the deep therapy of malignant tumors.

1. S.A. Maier. *Plasmonics: Fundamentals and Applications* (Springer Science & Business Media, 2007).
2. M. Hu, J. Chen, Z.Y. Li, L. Au, G.V. Hartland, X. Li, Y. Xia. Gold nanostructures: engineering their plasmonic properties for biomedical applications. *Chem. Soc. Rev.* **35**, 1084 (2006).
3. E.M. Larsson, C. Langhammer, I. Zorić, B. Kasemo. Nanoplasmonic probes of catalytic reactions. *Science* **326**, 1091 (2009).
4. H.A. Atwater, A. Polman. Plasmonics for improved photovoltaic devices. *Nat. Mater.* **9**, 205 (2010).
5. N.L. Dmitruk, S.Z. Malinich. Surface plasmon resonances and their manifestation in the optical properties of nanostructures of noble metals. *Ukr. Fiz. Zh. Ogl.* **9**, 3 (2014) (in Ukrainian).
6. D.J. De Aberasturi, A.B. Serrano-Montes, L.M. Liz-Marzán. Modern applications of plasmonic nanoparticles: from energy to health. *Adv. Opt. Mater.* **3**, 602 (2015).
7. B. Špačková, P. Wrobel, M. Bocková, J. Homola. Optical biosensors based on plasmonic nanostructures: a review. *Proc. IEEE* **104**, 2380 (2016).
8. V.I. Balykin, P.N. Melentiev. Optics and spectroscopy of a single plasmonic nanostructure. *Usp. Fiz. Nauk* **188**, 143 (2018) (in Russian).
9. M.M. Miller, A.A. Lazarides. Sensitivity of metal nanoparticle surface plasmon resonance to the dielectric environment. *J. Phys. Chem. B* **109**, 21556 (2005).
10. A.V. Korotun, A.A. Koval. Optical properties of spherical metal nanoparticles coated with an oxide layer. *Opt. Spektrosk.* **127** 1032 (2019) (in Russian).
11. A.V. Korotun, A.O. Koval, A.A. Kryuchyn, V.M. Rubish, V.V. Petrov, I.M. Titov. *Nanophotonic Technologies. Current State and Prospects* (FOP Sabov A.M., 2019) (in Ukrainian) [ISBN: 978-966-02-9059-4].
12. U. Kreibig, M. Vollmer. *Optical Properties of Metal Clusters* (Springer, 1995).
13. R. Ruppin, H.Yato. Size and shape effects on the broadening of the plasma resonance absorption in metals. *Phys. Status Solidi B* 74, 647 (1976).
14. N.I. Grigorchuk, P.M. Tomchuk. Optical and transport properties of spheroidal metal nanoparticles with account for the surface effect. *Phys. Rev. B* **84**, 085448 (2011).
15. G.N. Blackman III, D.A. Genov. Bounds on quantum confinement effects in metal nanoparticles. *Phys. Rev. B* **97**, 115440 (2018).
16. V.P. Kurbatskii, V.V. Pogosov. Low-frequency optical absorption by small metal particles. *Pis'ma Zh. Tekhn. Fiz.* **26**, 84 (2000) (in Russian).
17. V.P. Kurbatskii, A.V. Korotun, V.V. Pogosov. On the influence of the electron spectrum quantization of small metal particles on optical absorption in composites. *Zh. Tekhn. Fiz.* **82**, 130 (2012) (in Russian).

18. K. Tanabe. Field enhancement around metal nanoparticles and nanoshells: A systematic investigation. *J. Phys. Chem. C* **112**, 15721 (2008).
19. Yu.I. Petrov. *Clusters and Small Particles* (Nauka, 1986) (in Russian).
20. R. Sato, Ma. Ohnuma, K. Oyoshi, Y. Takeda. Experimental investigation of nonlinear optical properties of Ag nanoparticles: Effects of size quantization. *Phys. Rev. B* **90**, 125417 (2014).
21. K.N. Afanasev, I.A. Boginskaya, A.V. Dorofeenko, A.V. Gusev, K.A. Mailyan, A.V. Pebalk, V.N. Chvalun, S.A. Ozerin, M.V. Sedova, I.A. Rodionov, W.V. Pogosov, I.A. Ryzhikov. Poly(p-xylylene)silver nanocomposites: Optical, radiative, and structural properties. *IEEE Trans. Nanotechnol.* **16**, 274 (2017).
22. M.M. Moskovits, I. Srnová-Šloufová, B. Vlčková. Bimetallic Ag–Au nanoparticles: Extracting meaningful optical constants from the surface-plasmon extinction spectrum. *J. Chem. Phys.* **116**, 10435 (2002).
23. V.I. Belotelov, G. Carotenuto, L. Nicolais, A. Longo, G.P. Pepe, P. Perlo, A.K. Zvezdin. Online monitoring of alloyed bimetallic nanoparticle formation by optical spectroscopy. *J. Appl. Phys.* **99**, 044304 (2006).
24. M. Saliminasab, F. Shirzaditabar, R. Moradian. Electromagnetic field amplification in Al/Ag spherical nanostructures. *Appl. Phys. A* **124**, 870 (2018).
25. N. Valizade-Shahmirzadi, T. Pakizeh. Optical characterization of broad plasmon resonances of Pd/Pt nanoparticles. *Mater. Res. Express.* **5**, 04538 (2018).
26. S. Sompech, S. Thaomola, A. Chingsungnoen, T. Dasri. Theoretical calculation of optical absorption property of Cu@Ag core–shell composite nanoparticle. *Mater. Res. Express.* **6**, 026201 (2019).
27. A.V. Skidanenko, L.A. Avakyan, E.A. Kozinkina, L.A. Bugaev. An effect of internal structure of bimetallic nanoparticles on the optical properties of the AuAg/glass material. *Fiz. Tverd. Tela* **61**, 115 (2019) (in Russian).
28. M. Chen, S. Tang, Z. Guo, X. Wang, S. Mo, X. Huang, N. Zheng. Core–shell Pd@Au nanoplates as theranostic agents for in-vivo photoacoustic imaging, CT imaging, and photothermal therapy. *Adv. Mater.* **26**, 8210 (2014).
29. A.J. McGrath, Y.H. Chien, S. Cheong, D.A. Herman, J. Watt, A.M. Henning, R.D. Tilley. Gold over branched palladium nanostructures for photothermal cancer therapy. *ACS Nano* **9**, 12283 (2015).
30. G.P. Zograf, A.S. Timin, A.R. Muslimov, I.I. Shishkin, A. Nominé, J. Ghanbaja, P. Ghosh, Q. Li, Mikhail V. Zyuzin, S.V. Makarov. All-optical nanoscale heating and thermometry with resonant dielectric nanoparticles for controllable drug release in living cells. *Laser Photon. Rev.* **14**, 1900082 (2020).
31. H.C. van de Hulst. *Light Scattering by Small Particles* (Dover, 1981).
32. C.F. Bohren, D.R. Huffman. *Absorption and Scattering of Light by Small Particles* (Wiley, 2008) [ISBN:978-0-471-29340-8].
33. A.V. Babich, V.V. Pogosov. Effect of dielectric coating on the electron work function and the surface stress of a metal. *Surf. Sci.* **603**, 2393 (2009).
34. V.V. Pogosov. On some tenzoemission effects of the small metal particles. *Solid State Commun.* **81**, 129 (1992).
35. N.W. Ashcroft, N.D. Mermin. *Solid State Physics* (Saunders College Publishing, 1976).
36. G. Baffou, R. Quidant, F.J. Garcia de Abajo. Nanoscale control of optical heating in complex plasmonic systems. *ACS Nano* **4**, 709 (2010).

Received 07.07.20.
Translated from Ukrainian by O.I. Voitenko

А.В. Коротун, А.О. Коваль, В.В. Погосов

ОПТИЧНІ ХАРАКТЕРИСТИКИ
БІМЕТАЛЕВИХ НАНОКУЛЬ

В роботі одержано формулу для часу релаксації електронів на поверхні і проаналізовано частотну залежність електричної і магнітної компонент поляризовності двошарової металевої нанокулі. Максимуми поляризовності відповідають плазмонним резонансам ядра та оболонки. Розрахунки було проведено для біметалевих наночастинок Ag–Au, Au–Ag та Ag–Al, розташованих у тефлоні. Продемонстровано можливість керування оптичними характеристиками біметалевих наночастинок зміною їх морфології. Проведено розрахунки перерізів екстинкції і розсіювання та фактора підсилення поля в околі наночастинок у широкому спектральному інтервалі за різних співвідношень розмірів ядра та оболонки, а також оцінено температуру біметалевої нанокулі для фототермічної терапії злоякісних пухлин.

Ключові слова: біметалева наночастинка, дипольна поляризовність, діелектрична функція, поверхневий плазмон, фактор підсилення поля.